HEFAT2010
7th International Conference on Heat Transfer, Fluid Mechanics and Thermodynamics
19-21 July 2010
Antalya, Turkey

ANALYTICAL METHOD TO STUDY THE TEMPERATURE DISTRIBUTION OF A MOVING HEAT SOURCE ELECTRON BEAM MICRO-WELDING

Satya S. Gajapathi [a], Patricio. F. Mendez [b], Sushanta.K. Mitra* [a]
*Author for correspondence
[a] Department of Mechanical Engineering, [b] Department of Chemical and Materials Engineering
University of Alberta,
Edmonton, T6G2G8,
Canada,
E-mail: sushanta.mitra@ualberta.ca

ABSTRACT

Recently, the use of electron beam for micro-welding has become one of the primary research areas. Electron beam can behave as a volumetric heat source and is capable of traveling very fast and focusing at very small spot sizes. This proves ideal for welding at small scales as thermal stresses and losses due to ablation are controlled in the material. The choice of beam parameters remains a challenge as it depends on many factors like characteristics of the material and nature of application. An understanding of the beam-substrate interactions and hence the temperature distribution in the material due to this, can lead to wide spread applications of this technique. An analytical method based on the theory of heat transfer is proposed in the present work to yield the temperature distributions in the material during electron beam micro-welding. Plots identifying the maximum temperature and region of melting, obtained as results of the study, can help to optimize beam parameters for a process. The material properties of stainless steel are used to plot the temperature distribution in the material during micro-welding. The formulation is also extended to make use of electron beam for nano-welding, extrapolating the macro-level properties. For the case of nano-welding, the weld characteristics like the maximum temperature, weld depth and width are obtained for the specified values of the beam parameters, using the material properties of silicon.

INTRODUCTION

The ever-decreasing size of the electronic components, eg. microchips, pose a growing requirement of miniaturized features with high edge acuity and negligible thermal damage zone. Micro-welding is a key fabrication process utilized in the manufacture of miniature devices, including implantable medical devices and MEMS. Welding at micro-scale brings in new challenges in the form of surface ablation, capillary effects, etc. Also, the characteristics of the welds produced are very sensitive to the nature of application. The joining points have frequently a functional task, e.g., electrical conductivity or the sealing of the component. Hence, welding at micro-scales is restricted to the use of highly localized heat sources. Laser beams and electron beams, owing to their capability of focussing at small spot sizes and hence very high power density, are suitable for such purposes. While laser welding at micro scale is largely being used in industries, the use of electron beam technology is still in the laboratory stage.

NOMENCLATURE

A	[g/mol]	Atomic weight
c_p	[J/kg.K]	Specific heat capacity
d	[m]	Diameter of the electron beam
I	[I]	Probe current
k	[W/mK]	Thermal conductivity
l	[m]	Characteristic length along z-axis
Pe	[-]	Peclet number [vd/α]
q''	[W/m^2]	Heat flux
q'''	[W/m^3]	Volumetric heat generation
T	[^{0}C]	Temperature
t	[s]	Time
V	[V]	Accelerating voltage
v	[m/s]	Velocity
w	[m]	Power of the beam [V*I]
W	[W]	Characteristic length along y-axis
x	[m]	Cartesian axis direction
y	[m]	Cartesian axis direction
Z	[-]	Atomic number
z	[m]	Cartesian axis direction

Special characters

α	[m^2/s]	Thermal diffusivity
ρ	[kg/m^3]	Density
σ	[m]	Standard deviation of a Gaussian function

Subscripts

max	Maximum
0	Ambient or reference
f	Final
m	Melting
s	On the surface along y-axis
t	As a function of time

The properties like realisation of small spot size, inertia free manipulation, concentrated volumetric energy input and applicability to metals, insulators and semiconductors makes

the use of electron beam welding technique very promising for micro systems compared to use of laser beam. However, electron beam welding machines from the macro range cannot be used in the micro scales because of their large beam spots and lack of motion control. With the growing necessity of microprocessing technology, scanning electron microscope (SEM), which otherwise is used for surface measurement or characterization, is modified to produce a high-density localized electron beam suitable for microjoining [1,2]. Smolka et al. [3] studied the characteristics of the SEM as micro-welding machine. Knorovsky et al. [4] evaluated the effects of various factors related to heat transfer and energy absorption on the parameter selection of a SEM for micro-welding operations. A review of difficulties and prospects in using a SEM for micro-welding for various kinds of materials are reported by Reisgen et al. [5]. The parameters of electron beam for micro-welding of steel wires are reported experimentally by Reisgen et al. [6].

Other than the difficulties in controlling SEM parameters, the success of the electron beam technology in micro-welding is limited because of a lack of thorough understanding of the heat transfer taking place at this scale. The challenge is to model the rapidly scanning electron beam as a heat source. Monte Carlo simulations have been carried out to characterize the electron beam as volumetric heat source [4,7]. The size of the beam interaction volume is studied to be a function of accelerating voltage and the material properties like atomic weight and atomic number [8,9]. Hwang et al. [10] developed a semi-empirical method to model the heat source. Basing on this, bead-on-plate experiments for a stainless steel are carried out for different combinations of beam parameters like beam current and beam velocity.

An efficient way to predict the beam parameters for a micro-welding operation would be to carry out heat transfer analysis and optimize the variables by studying the temperature distributions, which hasn't been carried out at these scales to the best of author's knowledge. In the present study, an analytical method is proposed to study the temperature distributions in the material due to the energy transfer from the beam. The model considers electron beam as moving volumetric heat source. The parameters of the beam are required to be fixed in such a way that only a small region is melted around the heat source and negligible amount of evaporation is taking place. The beam parameters like voltage input, probe current, beam diameter, and beam velocity are required to predict the temperature distribution in the material. Beam voltage is fixed based on the depth of the weld required [8,9]. The beam diameter is fixed according to the scale of welding required. Heat input (power/velocity) is selected in such a way that the required temperature distribution is obtained with less thermal stress zone. Present study is based on the general energy conservation principle that applies to all materials at all scales. The heat source model proposed by Mendez et al. [11] is used to represent the electron beam.

ANALYSIS

Electron beam is studied as heat source which generates heat in a concentrated volume near the surface. This causes an increase in enthalpy in the regions near the hot spots. The Fourier heat conduction equation including the source term is required to be solved in the material to obtain temperature distribution.

$$k\left(\frac{\partial T^2}{\partial x^2}+\frac{\partial T^2}{\partial y^2}+\frac{\partial T^2}{\partial z^2}\right)+q'''=\rho c_p\frac{\partial T}{\partial t} \quad (1)$$

For welding at micro-scales, the heat source needs to move very fast over the surface. This is to avoid concentration of heat at any single point, which otherwise can increase thermal stress in the material or increased loss of volume due to evaporation. The Peclet number (Pe) is high for such fast moving heat sources. Thus, heat dissipation due to conduction can be neglected for high Pe, taking into account the small time scales [11]. Hence, the Fourier heat conduction equation is reduced to heating rate equation as,

$$\rho c_p\frac{\partial T}{\partial t}=q''' \quad (2)$$

Equation (2) is solved over a semi-infinite solid. A 3-D block around the heat source at a given point of time is represented in Fig. 1. The region of sharp temperature gradients is however restricted to a small region around the heat source, depending on the heat input and beam diameter. Heat loss due to radiation and evaporation from the top boundary is purposefully neglected in this study so that a distribution of maximum temperature at any point is obtained. It is the knowledge of maximum temperature which is predominant while selecting the beam parameters as it helps to control the process.

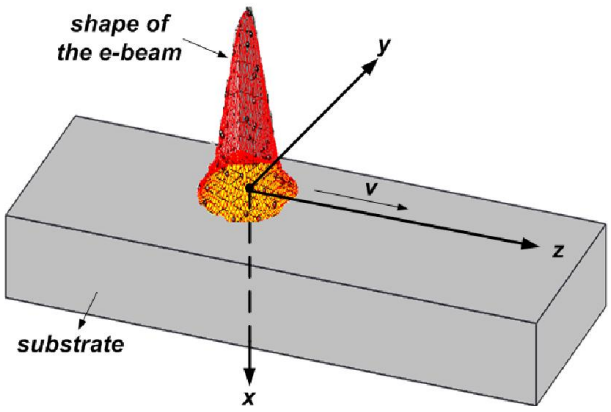

Figure 1 Model of a semi-infinite solid showing the moving heat source and the coordinate axes ($0<x<\infty,-\infty<y<\infty,-\infty<z<\infty$)

Introducing the following dimensionless variables:

$$x^*=x/x_e \quad (3)$$

The characteristic length x_e along the depth is defined as the electron penetration depth and is given by the Kanaya-Okayama relationship [8], for a given accelerating voltage and properties of the material.

$$y^*=y/w \quad (4)$$

$$z^*=z/l \quad (5)$$

In the stationary coordinate frame as the source is moving along z-direction, it position can be defined as a function of time as:

$$z=vt \quad (6)$$

By using eq. (5)

$$t = \frac{l}{v} z^* \tag{7}$$

The normalized time variable is defined as, $t^* = z^*$,

$$t = \frac{l}{v} t^* \tag{8}$$

The temperature and the source term used in the heating rate equation can be written in the normalized form as:

$$T(x, y, z) = T_0 + \Delta T_{\max} T^*(x^*, y^*, z^*(t^*)) \tag{9}$$

$$q'''(x, y, z(t)) = q'''_{\max} q^*(x^*, y^*, z^*(t^*)) \tag{10}$$

Non-dimensional form of Eq. (2) is written as:

$$\rho c_p \frac{\Delta T_{\max}}{l/v} \frac{dT^*}{dt^*} = q'''_{\max} q^* \tag{11}$$

In an electron beam welding process, the power of the beam is converted in to thermal energy as the electrons collide with the material. The energy conservation principle provides the relationship between the volumetric heat input and the power of the beam.

$$\int_v q''' dv = V.I \tag{12}$$

$$\int_{-\infty}^{\infty}\int_{-\infty}^{\infty}\int_{0}^{\infty} q''' dx dy dz = W \tag{13}$$

Equation (13) can also be written in normalized form as:

$$q'''_{\max} x_e w l \int_{-\infty}^{\infty}\int_{-\infty}^{\infty}\int_{0}^{\infty} q^* dx^* dy^* dz^* = W \tag{14}$$

All the power of the beam is not converted into heat. There is loss of power during this process due to back scattered electrons, X-rays, etc. Usually there is an efficiency factor involved to calculate the actual power from the theoretical power input.

Heat Source Modelling

The shape of the volumetric heat source is assumed to be a round Gaussian distribution with an exponential decay penetration, as proposed by Mendez et al [11].

$$q'''(x, y, z) = q'''_{\max} e^{-\left(\frac{y^2+z^2}{2\sigma^2}\right)} e^{-\left(\frac{x}{x_e}\right)} \tag{15}$$

Equation (15) can be written in the non-dimensional form as:

$$q^*(x^*, y^*, z^*) = e^{-\left(\frac{y^{*2}+z^{*2}}{2}\right)} e^{-x^*} \tag{16}$$

The characteristic lengths along y and z directions (l and w respectively) are defined here as the standard deviation of the Gaussian function. The Gaussian function is characterized by its full width half maximum (FWHM=2.335σ), which is reported as diameter of the electron beam.

SOLUTION

The heat source term can now be integrated all over the domain to find the maximum volumetric heat input using Eq. (14) as:

$$q'''_{\max} x_e w l \int_{-\infty}^{\infty}\int_{-\infty}^{\infty}\int_{0}^{\infty} e^{-\left(\frac{y^2+z^2}{2\sigma^2}\right)} e^{-\left(\frac{x}{x_e}\right)} dx^* dy^* dz^* = W \tag{17}$$

$$\int_{-\infty}^{\infty}\int_{-\infty}^{\infty}\int_{0}^{\infty} e^{-\left(\frac{y^2+z^2}{2\sigma^2}\right)} e^{-\left(\frac{x}{x_e}\right)} dx^* dy^* dz^* = 2\pi \tag{18}$$

Using Eqs. (17) and (18),

$$q'''_{\max} = \frac{W}{2\pi x_e w l} \tag{19}$$

The maximum temperature is expected to be obtained on the z-axis along the path of the source (x=0 and y=0). This can be calculated using Eq. (16) in Eq. (11) and by integrating over the entire time range.

$$\rho c_p \Delta T_{\max} \frac{v}{l} \int_0^{T^*_{\max}} dT^* = q'''_{\max} \int_{-\infty}^{\infty} e^{-\left(\frac{z^{*2}}{2}\right)} dt^* \tag{20}$$

$$\rho c_p \Delta T_{\max} \frac{v}{l} = q'''_{\max} \sqrt{2\pi} \tag{21}$$

For maximum temperature, $T^*_{\max}$=1. Substitution of Eq. (19) in Eq. (21) provides the expression for maximum temperature attained during the operation.

$$T_{\max} - T_0 = \frac{W}{\sqrt{2\pi} v x_e w} \tag{22}$$

Calculation of final temperature distribution along *y*-direction on *x*=0 plane

Using Eqs. (16) and (11) to integrate over the entire time range, the final temperature distribution due to the input heat in the x=0 plane is obtained as:

$$\rho c_p \Delta T_{\max} \frac{v}{l} \int_0^{T_f^*} dT^* = q'''_{\max} e^{-\left(\frac{y^{*2}}{2}\right)} \int_{-\infty}^{\infty} e^{-\left(\frac{z^{*2}}{2}\right)} dt^* \tag{23}$$

$$\rho c_p \frac{v}{l} (\Delta T_{\max} T^*) = q'''_{\max} e^{-\left(\frac{y^{*2}}{2}\right)} \sqrt{2\pi} \tag{24}$$

Equation (24) can be simplified using Eqs. (9) and (21) as

$$T = T_0 + \Delta T_{\max} e^{\left(-\frac{y^{*2}}{2}\right)} \tag{25}$$

The heat flux distribution along y-axis on the x=0 plane is calculated by substituting x=0 in Eq. (15) and integrating along z-axis.

$$q_s = q_{\max} e^{-\left(\frac{y^2}{2\sigma^2}\right)} \int_{-\infty}^{\infty} e^{-\frac{z^2}{2\sigma^2}} dz \tag{26}$$

$$q_s = \sqrt{2\pi}\sigma q_{\max} e^{-\left(\frac{y^2}{2\sigma^2}\right)} \quad (27)$$

Calculation of melting isotherm in *x-y* plane

The depth and width of the weld are approximated by calculating the region in the *x-y* plane bounded by the melting temperature isotherm. The temperature has been fixed as the melting point of the material and the locus of points having melting temperature (x_m and y_m) is calculated by integrating Eq. (11) over time.

$$\rho c_p \Delta T_{\max} \frac{v}{l} \int_0^{T_m^*} dT^* = q'''_{\max} e^{-\left(\frac{{y_m}^{*2}}{2}\right)} e^{-x_m^*} \int_{-\infty}^{\infty} e^{-\left(\frac{t^{*2}}{2}\right)} dt^* \quad (28)$$

In Eq. (28), x_m and y_m are are the melting depth and melting width for any given point along the path of the moving heat source. They are calculated based on the final temperature attained as the source moves all along the semi-infinite solid. Also, z^* has been substituted as t^* in Eq. (28) as they are analogous.

$$\rho c_p \Delta T_{\max} \frac{v}{l} {T_m}^* = \sqrt{2\pi} q'''_{\max} e^{-\left(\frac{{y_m}^{*2}}{2}\right)} e^{-x_m^*} \quad (29)$$

Equation (29) can be simplified using Eqs. (9) and (21) as :

$$\frac{\Delta T_m}{\Delta T_{\max}} = e^{\left(-\frac{{y_m}^{*2}}{2} - x_m^*\right)} \; or \; \frac{x_m}{x_e} + \frac{{y_m}^2}{2\sigma^2} = \ln \frac{\Delta T_{\max}}{\Delta T_m} \quad (30)$$

Calculation of melting isotherm in *y-z* plane

Melting isotherms can also be found in the *y-z* plane by substituting $x^*=0$, $y^*={y_m}^*$ and $z = {z_m}^*$ in Eq. [28] and integrating in the range of z^*.

$$\rho c_p \Delta T_{\max} \frac{v}{l} \int_0^{T_m^*} dT^* = q'''_{\max} e^{-\left(\frac{{y_m}^{*2}}{2}\right)} \int_{-\infty}^{z_m^*} e^{-\left(\frac{{z_m}^{*2}}{2}\right)} dz^* \quad (31)$$

Using eqs. (9) and (21),

$$\frac{\sqrt{2\pi}\Delta T_m}{\Delta T_{\max}} = e^{-\left(\frac{{y_m}^2}{2\sigma^2}\right)} \int_{-\infty}^{z_m^*} e^{-\left(\frac{{z_m}^{*2}}{2}\right)} dz^* \quad (32)$$

The value of $\Delta T_{\max}$ can be found using Eq. 22 and hence Eq. 32 can be used to plot the melting isotherm in the *y-z* plane.

Calculation of Temperature Distribution Along z-direction

The temperature variation at a point on the path of the moving heat source can be calculated as the heat source moves over it. This is analogous to calculating the temperature along z-axis at fixed point of time. On *z*-axis, Eq. (20) can be written as:

$$\rho c_p \Delta T_{\max} \frac{v}{l} \int_0^{T_{\max}^*} dT^* = q'''_{\max} \int_{-\infty}^{t^*} e^{-\left(\frac{t^{*2}}{2}\right)} dt^* \quad (33)$$

For final temperature along z-axis, Eq. (33) can be solved by substituting Eqs. (9) and (21):

$$T = T_0 + \frac{\Delta T_{\max}}{\sqrt{2\pi}} \int_{-\infty}^{t^*} e^{\left(-\frac{t^{*2}}{2}\right)} dt^* \quad (34)$$

The heat flux as a function of time can be calculated over a point on the path of the heat source (*z*-axis) by substituted x=0 and integrating all over the *y*-axis in Eq. (15) as:

$$q_t = \sqrt{2\pi} q_{\max} e^{-\left(\frac{(vt)^2}{2\sigma^2}\right)} \quad (35)$$

RESULTS AND DISCUSSIONS

The analytical expression obtained for temperature and heat flux depends on the properties of the material used and beam parameters. Also, selection of beam parameters for welding depends on the material properties. The density of the material decides the electron penetration depth based on the accelerating voltage. The properties of the stainless steel and silicon, relevant to the welding operation using electron beam, are shown in Table 1.

Table 1 Properties of Stainless Steel and Silicon

Properties	Steel(μ-welding)	Silicon (nano-welding)
k	33	163
ρ	7912	2330
c_p	468	703
T_m	1400	1414
T_0	25	25
A	52	28
Z	26	14

The four pre-dominant characteristics of an electron beam used in welding at small scales-accelerating voltage, probe current, beam diameter, and beam velocity are specified in Table 2. The beam voltage depends on the amount of penetration required i.e., the weld depth. Generally, a penetration depth of the same order of beam diameter or smaller is preferred. The beam diameter is selected according to the scale of the material to be joined. The maximum temperature has been approximated for several cases of heat input (power/velocity) and the results are illustrated for the most optimized set of beam parameters. It has to be observed that the maximum temperature obtained for a set of beam parameters shouldn't exceed the melting temperature by a large limit.

Table 2 Beam parameters used

Beam parameters	Steel(μ-welding)	Silicon (nano-welding)
V	50 [KV]	3 [KV]
I	200[μA]	10 [nA]
FWHM	12 [μm]	100 [nm]
v	25 [m/s]	0.7 [m/s]

Beam power is the product of the accelerating voltage and the probe current. Kanaya-Okayama relationship [8] is used to calculate the maximum electron penetration depth (x_e) using the accelerating voltage, atomic number and mass of the material. x_e gives an idea of the depth in the substrate through which

electrons from the beam losses its energy and hence this is of the same order as of the melting depth. Table 3 presents the intermediate parameters calculated to estimate the final temperature distribution.

Table 3 Intermediate parameters

	Steel(μ-welding)	Silicon (nano-welding)
W	10 [W]	30e-06 [W]
x_e	2.99 [μm]	86.4 [nm]
α	8.9e-06 [m^2/s]	9.95e-05 [m^2/s]

In Figure 2, temperature variation along y-axis (perpendicular to the direction of heat source motion) is plotted for any given point on the z-axis (on the path of the heat source) using Eq. 25. Heat flux distribution along the same line is found out using Eq. 27and shown in the plot. The temperature and the heat flux have their peaks at y=0 i.e, along the centreline of the surface. The temperature gradients become negligible for lengths of about 20μm away from the centre line along y-axis.

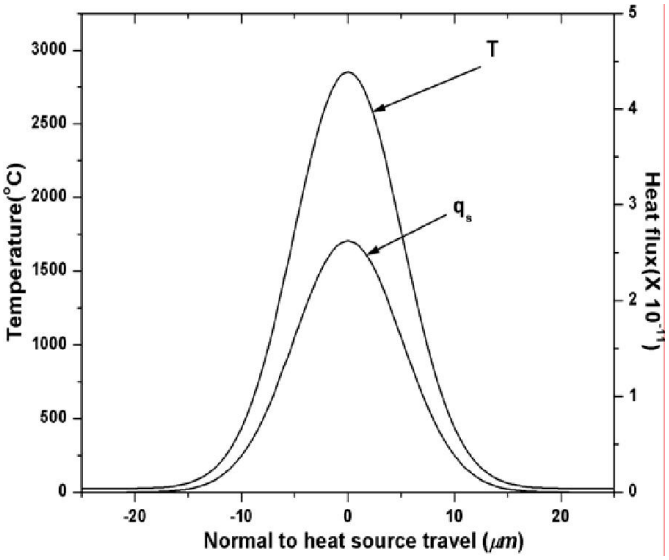

Figure 2 Variation of temperature and heat flux along y-axis for any given point on the z-axis on the steel surface.

Figure 3 shows the melting temperature isotherm, using Eq. (30). The region of melting as the heat source over a point is shown. The position of the beam is represented by plotting the heat flux distribution along y-axis using Eq. (27). The maximum depth of melting (x_m) is obtained right under the beam. The points of intersection of the melting temperature isotherm on y-axis represent the maximum width of the weld.

Figure 4 shows the melting temperature isotherm as seen on the top surface (y-z plane) using Eq. (32). The heat source is located at the origin. Sharp gradient in the slope of the melting isotherm near the origin is due to the high velocity of the heat source. Away from the origin, the curves rise normal to the horizontal axis. The intercept represents the weld width. The melting isotherm extends a small length scale below the origin. This represents the melting region ahead of the heat source. The outer circle represents the spot size and the position of the beam. The diameter of the circle is the FWHM value of the Gaussian function chosen to represent the electron beam.

$$y^2 + z^2 = \left(\frac{d^2}{4}\right) \tag{36}$$

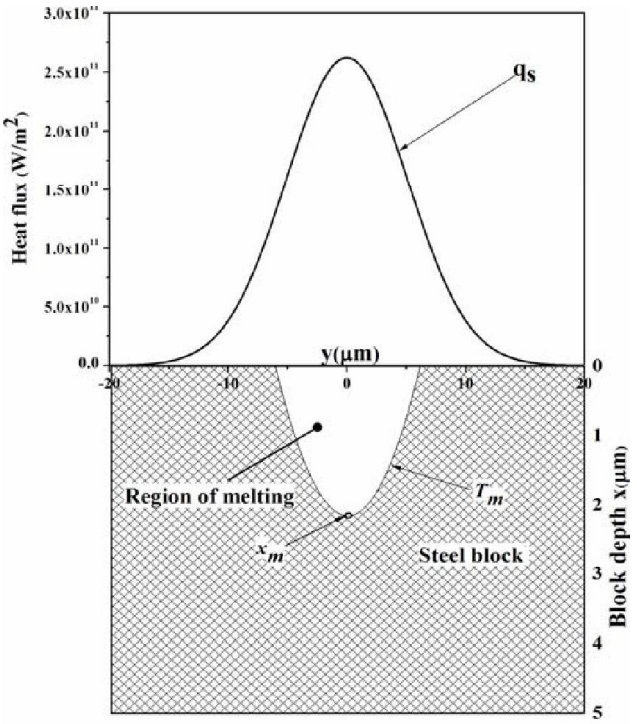

Figure 3 Isotherm of melting temperature in the x-y plane. Heat flux distribution along y-axis is also shown.

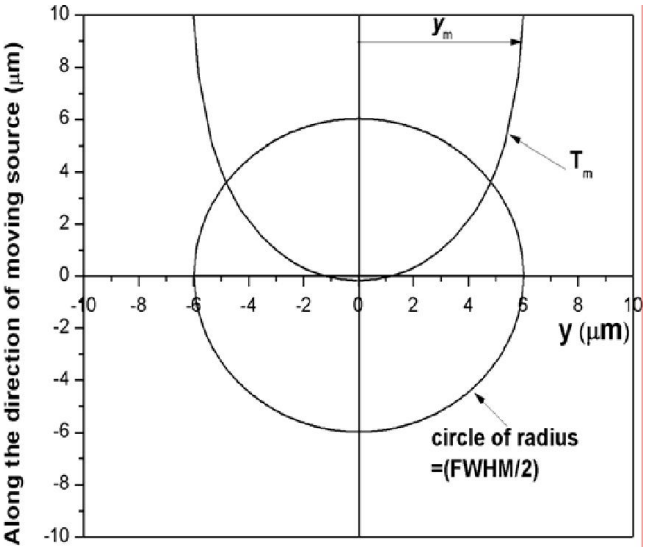

Figure 4 Isotherm of melting temperature in the y-z plane of the steel surface.

Figure 5 shows the variation of temperature with time over any given point along the path of the heat source. The

temperature of the point begins to increase as the heat source arrives at a closer proximity. Time zero signifies that the beam is over head of the chosen point. It is noticed that the melting temperature (1400 ^{0}C) is attained before the heat source arrives on the point. This small time advance corresponds to the melting length below origin in Fig. 3. Also, it is found that the maximum temperature at the point is attained after the heat source has moved a small distance beyond it.

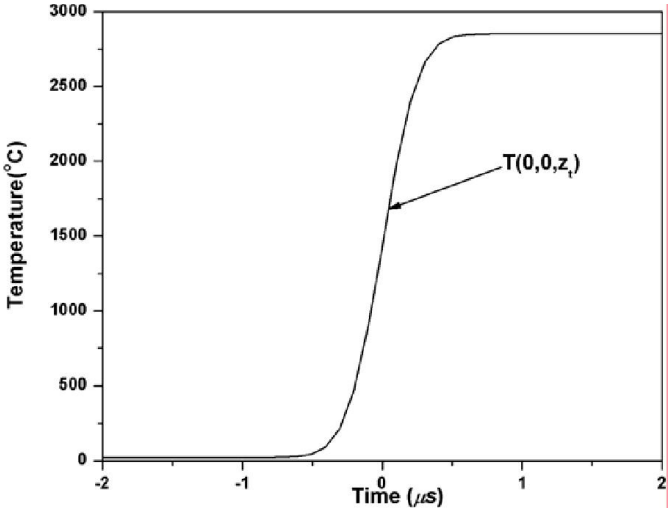

Figure 5 Variation of temperature at a point on the steel surface along the path of the moving heat source.

The maximum temperature obtained during the micro-welding process for the specified set of beam parameters is 2853 ^{0}C as suggested by the peak value of temperature plot in Figs. 2 and 3. The farthest point of melting temperature along *x*-axis and *y*-axis in Fig. 3 represents the weld depth and weld width, respectively. The weld width can also be compared by measuring the distance along *y*-axis of the melting isotherm in Fig. 4 far away from the origin. The values of these parameters as obtained from the plots are shown in Table 4 for micro-welding of steel.

This technique can further be extended to weld materials whose characteristic dimensions are in nanometers (nm). The weld characteristics of nano-welding for silicon are obtained from Eqs. (22) and (30) and the corresponding parameters are provided in Table 4.

Table 4 Weld characterstics

	Steel(μ-welding)	Silicon (nano-welding)
T_{max}	2853 [^{0}C]	2871 [^{0}C]
x_m	2.16 [μm]	62 [nm]
y_m	6.2 [μm]	50.9 [nm]

CONCLUSION

Electron beam has been studied as volumetric heat source that can be used efficiently for welding at lower scales. A mathematical model has been developed to find the temperature distributions during welding operation using such a beam. A detailed procedure has been outlined to interpret the results, in the form of maximum temperature on the surface and melting region, which guides the selection of beam parameters.

Use of high powered electron beam source moving on the surface of the substrate at very high velocity is identified as the most efficient way to achieve welding at low scales. It is also observed that for very short scales of distance and time, the temperature away from the heat source reaches the steady state. The possibility of using such a beam for nano-welding is also demonstrated.

REFERENCES

[1] Dilthey U., Dorfmuller T., Micro electron beam welding, *Microsystem. Technologies,*12, 2006, pp. 626-631

[2] Knorovsky, G.A., Nowak-Neeley, B.M., Holm, E.A., Microjoining with a Scanning Electron Microscope, *Science and Technology of Welding and Joining*, Vol. 11, No.6, 2006, pp. 641-649

[3] Smolka G., Gillner A., Bosse L., Lutzeler R., Micro-electron beam welding and laser machining-potentials of beam welding methods in the micro-system technology, *Microsystem. Technologies,*10, 2004, pp. -187-192

[4] Knorovsky, G.A., MacCallum, D.O., Meyers, M.T., Selection of Parameters for μE-Beam Welding, *Science and Technology of Welding and Joining*, Vol. 11, No 6, 2006 , pp. 672-680

[5] Reisgen U., Dorfmuller T., Developments in micro-electron beam welding, *Microsystem. Technologies,*14, 2008, pp. 1871-1877

[6] Reisgen U., Dorfmuller T., Micro-electron beam welding with a modified scanning electron microscopy: Findings and prospects, *J. Vac. Sci. Technol,*B 27(3), 2009, pp. 1310-1314

[7] Gauvin, R., Drouin, D., Couture, A.R., Casino v2.42, available at www.gel.usherb.ca/casino/

[8] Kanaya K., Okayama S., Penetration and energy-loss theory of electrons in solid targets, *J. Phys. D: Appl. Phys.,* vol.5, 1972, pp. 43-58

[9] Schwarz H., Mechanism of high-powered-density electron beam penetration in metal, *J. Appl. Phy.,* vol. 35(7), pp. 2020-2029

[10] Il-Han Hwang, Suck-Joo Na, A study on heat source modeling of scanning electron microscopy modified for material processing, *Metallurgical and materials transactions B,* vol. 36B, 2005, pp. 133-139

[11] Mendez, P. F., Clevenger J., Brown, S., Electron beam welding method and apparatus using controlled volumetric heating, US Patent No. 2006/0102597 A1 (2006).